Published in final edited form as:
Anal Chem. 2014 January 21; 86(2): 1045–1052. doi:10.1021/ac402230h.

In Vivo Proton–Electron Double-Resonance Imaging of Extracellular Tumor pH Using an Advanced Nitroxide Probe

Alexandre Samouilov[†,§], **Olga V. Efimova**[†], **Andrey A. Bobko**[†,‡], **Ziqi Sun**[†], **Sergey Petryakov**[†], **Timothy D. Eubank**[†,‡], **Dmitrii G. Trofimov**[‖], **Igor A. Kirilyuk**[‖], **Igor A. Grigor'ev**[‖], **Wataru Takahashi**[†,⊗], **Jay L. Zweier**[†,§], and **Valery V. Khramtsov**[†,‡,*]

[†]The Dorothy M. Davis Heart and Lung Research Institute, The Ohio State University, Columbus, Ohio 43210, United States

[‡]Division of Pulmonary, Allergy, Critical Care, and Sleep Medicine, The Ohio State University, Columbus, Ohio 43210, United States

[§]Division of Cardiovascular Medicine, Department of Internal Medicine, The Ohio State University, Columbus, Ohio 43210, United States

[‖]Vorozhtsov Institute of Organic Chemistry, Novosibirsk 630090, Russia

[⊗]Hokkaido University, Sapporo, Hokkaido 060-0814, Japan

Abstract

A variable radio frequency proton–electron double-resonance imaging (VRF PEDRI) approach for pH mapping of aqueous samples has been recently developed (Efimova et al. *J. Magn. Reson.* **2011**, *209*, 227–232). A pH map is extracted from two PEDRI acquisitions performed at electron paramagnetic resonance (EPR) frequencies of protonated and unprotonated forms of a pH-sensitive probe. To translate VRF PEDRI to an *in vivo* setting, an advanced pH probe was synthesized. Probe deuteration resulted in a narrow spectral line of 1.2 G compared to a nondeuterated analogue line width of 2.1 G allowing for an increase of Overhauser enhancements and reduction in rf power deposition. Binding of the probe to the cell-impermeable tripeptide, glutathione (GSH), allows for targeting to extracellular tissue space for monitoring extracellular tumor acidosis, a prognostic factor in tumor pathophysiology. The probe demonstrated pH sensitivity in the 5.8–7.8 range, optimum for measurement of acidic extracellular tumor pH (pH_e). *In vivo* VRF PEDRI was performed on Met-1 tumor-bearing mice. Compared to normal mammary glands with a neutral mean pH_e (7.1 ± 0.1), we observed broader pH distribution with acidic mean pH_e (6.8 ± 0.1) in tumor tissue. In summary, VRF PEDRI in combination with a newly developed pH probe provides an analytical approach for spatially resolved noninvasive pH_e monitoring, *in vivo*.

[*]**Corresponding Author**. valery.khramtsov@osumc.edu.

ASSOCIATED CONTENT

S Supporting Information

Additional details of **Im6** synthesis and spin echo sequence and experimental parameters. This material is available free of charge via the Internet at http://pubs.acs.org.

The authors declare no competing financial interest.

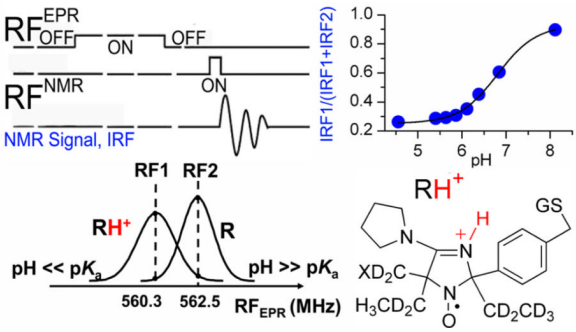

Acidity, or pH, is one of the most important parameters in the physiology of living organisms. On the tissue level, extracellular (pH_e) and intracellular (pH_i) pH values are tightly controlled to maintain optimal functionality. Aberration of normal tissue pH homeostasis in the human body has been reported for a number of pathological conditions that include cancers,[1,2] myocardial[3,4] and brain ischemia,[5,6] and chronic pulmonary[7] and kidney diseases.[8] Therefore, *in vivo* pH imaging can contribute to the diagnosis, understanding of disease progression, and treatment optimization.

The extracellular tumor tissue acidosis has been identified as a significant factor in cancer pathophysiology contributing to tumor initiation, progression, and therapy.[1] The imaging techniques currently employed for assessment of tumor pH_e include optical imaging, positron emission tomography (PET), magnetic resonance spectroscopy and imaging (MRI), and EPR imaging (EPRI). Optical imaging techniques allow for *in vivo* 3D pH mapping in small animals[1,9] but suffer from limited penetration depth. pH mapping using PET requires application of radioisotope labeled pH probes,[10] which is an obvious disadvantage relative to nonionizing magnetic resonance imaging techniques. Both MRI and low-frequency EPRI allow for *in vivo* applications in animals and humans due to sufficient depth of radio frequency microwaves penetrating living tissue. Nevertheless, measurement of pH_e provides a challenge for widely used ^{31}P NMR, which reports pH_i but is practically insensitive to pH_e[11] due to a higher concentration of intracellular inorganic phosphate. Therefore, MRI and NMR techniques for the assessment of tumor pH_e rely entirely on extracellular-targeted pH probes such as the ^{31}P pH probe 3-aminopropylphosphate, ^{19}F pH probes triflouromethylated pyridoxal derivative, and ZK-150471[11] and hyperpolarized ^{13}C-labeled bicarbonate.[12] While the use of hyperpolarized bicarbonate-^{13}C is considered as a potential approach for *in vivo* pH mapping in humans,[12] its practical application is limited by a short image acquisition time due to the fast ^{13}C signal decay. EPR-based pH mapping using nitroxide pH probes[13,14] possesses a high signal specificity due to the lack of endogenous paramagnetic species. However, pH mapping using continuous wave EPRI requires a long acquisition time and is hardly possible using available pH-sensitive probes that have short half-life *in vivo*. Moreover, short relaxation time of the nitroxide pH probes compromises spatial resolution of EPRI which requires the application of powerful field gradients and/or extraordinary fast pulse techniques.

Proton–electron double-resonance imaging (PEDRI) is based on the proton MRI acquired upon EPR irradiation of paramagnetic molecules,[15] the latter providing an enhancement of the NMR signal via transfer of polarization from electrons to protons by the Overhauser effect.[16] PEDRI has been shown to be a useful technique to image paramagnetic probe distribution[17–19] and tumor oximetry[20] in live animals. However, a conventional PEDRI approach lacks EPR spectral information. Recently developed functional PEDRI approaches, namely, variable field[21] and variable radio frequency (VRF)[22] PEDRI, allow for recovering essential spectral information and functional mapping. In the case of VRF

PEDRI pH mapping, a pH map is obtained from two PEDRI acquisitions performed at EPR frequencies of protonated and unprotonated forms of a pH-sensitive probe.[22] In this case, it is important to have paramagnetic probes with high aqueous solubility, pH sensitivity in the physiological range, and *in vivo* half-life of a few minutes or longer, sufficient for image data acquisition.

Imidazoline (**Im**) and imidazolidine (**In**) radicals have been proven to be useful stable paramagnetic probes for EPR spectroscopy and imaging of pH due to the large spectral effect upon protonation of atom N-3 of radical heterocycle and the large number of available structures.[13,23,24] Table 1 demonstrates the structures of the pH-sensitive nitroxides **In1**, **In2**, **Im1**, **Im3**, and **Im4** previously used in PEDRI experiments in live animals. Low pK_a values of these probes do not allow for their use in pH studies in tissue with pH homeostasis close to neutral. Nevertheless, they have been used for monitoring acidic pH values in the stomach of live rats.[18,24,25] Among these radicals, **Im4** has demonstrated the most advanced properties.[18] Bulky groups in the vicinity of the NO fragment enhanced **Im4** stability toward reduction and its half-life *in vivo* allowing for the monitoring of drug-induced stomach alkalinization and subsequent normalization of stomach acidity over 60–90 min. The presence of hydrophilic amino, pyridine, and hydroxy groups in the structure of **Im4** probe enhances its aqueous solubility and prevents its diffusion into biomembranes and redistribution from the stomach into surrounding tissues, as supported by PEDRI mapping.[18] The presence of protonatable pyridine group in the **Im4** structure in addition to protonatable nitrogen N-3 of radical heterocycle results in an extended range of its pH sensitivity from 1.7 to 5.8. However, the **Im4** probe still lacks pH sensitivity in the range above pH 6 required for pH assessment in most tissues, including slightly acidic tumors[1] or ischemic myocardium.[4] The **Im2** probe with pK_a 6.1 (Table 1) has been proposed for some time as more appropriate for pH studies in the physiological pH range[26] and has been recently used for pH mapping of aqueous samples using PEDRI[21,22] *in vitro*. Nevertheless, low sensitivity of the **Im2** probe to pH above 7 and a comparatively fast reduction with a half-life in living tissue of about 1 min or less[27] makes its *in vivo* application problematic.

In summary, the available paramagnetic pH probes explored for PEDRI measurements do not possess the required pH sensitivity in the physiological pH range (**In1**, **In2**, **Im1**, **Im3**, and **Im4**) and often demonstrate insufficient stability *in vivo* (**Im1** and **Im2**). In this work, the probe structure was optimized to improve the range of pH sensitivity, spectral properties, probe stability, and extracellular targeting enabling the *in vivo* PEDRI measurements of pH_e in tumor tissue.

MATERIALS AND METHODS

Synthesis

The deuterated pH-sensitive nitroxide, **Im6**, was synthesized as described below according to Scheme 1 (for the synthetic details and characterization of the compounds see the Supporting Information).

Hydroxyaminoketone 5

3-Hydroxyamino-3-ethylpentan-2-one hydrochloride-D_6 (**5**) was prepared using a simplified and improved previously published procedure.[28] The compound **5** has on average six deuterium atoms in the Et_2C moiety as a result of statistical distribution of the CD_3 groups. The crystalline precipitate of hydroxyaminoketone **5** hydrochloride was obtained with the overall yield 7.5 g (44.5%).

Nitrone 7

2-(4-Hydroxymethylphenyl)-4,4-diethyl-5-methyl-4H-imidazole 3-oxide-D_6 (**7**) was prepared using an optimized general procedure for synthesis of 1-hydroxy-2,5-dihydro-1*H*-imidazoles[29] and a mild method of oxidation of **6** to get a higher yield of **7** (3.8 g, 90%).

Oxime 8 and Amidine 10

2-(4-(Hydroxymethyl)phenyl)-4,4-diethyl-4H-imidazole-4-carbaldehyde oxime 3-oxide-D_6 (**8**) and 2-(4-hydroxymethylphenyl)-4,4-diethyl-5-pyrrolidino-4H-imidazole 3-oxide-D_6 (**10**) were synthesized as crude products with the yields 3.7 g (88%) and 1.3 g (60%), correspondingly, and were used in the next step without further purification.

Nitroxide 11

2-(4-(Hydroxymethyl)phenyl)-5,5-dimethyl-4-pyrrolidino-2-ethyl-2,5-dihydro-1H-imidazole-1-oxyl-D_{11} (**11**) was synthesized as follows. A C_2D_5MgBr solution prepared from C_2D_5Br (4 mL, 53 mmol) and Mg (1.5 g) in 40 mL of diethyl ether was slowly added dropwise under argon to a stirred suspension of **10** (1.3 g, 4.0 mmol) in a mixture of dry THF (20 mL), dry diethyl ether (50 mL), and dry benzene (50 mL). At the beginning of the addition, a fine precipitate is generated which forms a lump and is then dissolved with a clear solution formation. The reaction mixture was allowed to stand overnight. Then brine (15 mL) was added dropwise while stirring vigorously. The organic phase was separated and water solution extracted with EtOAc. The combined organic extracts were dried with anhydrous Na_2CO_3 and then bubbled with air for 24 h. The solvent was removed in vacuum. The nitroxide **11** was isolated from the residue by column chromatography on Al_2O_3, eluent $CHCl_3$. Yield 1.30 g (90%).

Spin Label RCl

2-(4-(Chloromethyl)phenyl)-2,5,5-triethyl-4-(pyrrolidino)-2,5-dihydro-1H-imidazol-1-oxyl hydrochloride-D_{11} (**RCl**) was synthesized as follows. Methanesulfonyl chloride (0.5 mL, 6.5 mmol) was added dropwise to a solution of nitroxide **11** (1 g, 2.8 mmol) in dry chloroform (5 mL) while stirring. Then triethylamine (0.4 mL, 2.9 mmol) was added dropwise, and the reaction mixture was stirred for ~2 h. The TLC analysis of the reaction mixture (silica gel 60 F_{254}, eluent $CHCl_3$) shows a gradual conversion of **11** into mesylate **12** (R_f ~ 0.8). Then the solvent was removed under reduced pressure, the residue was shaken with diethyl ether (30 mL) and a saturated solution of $NaHCO_3$ (10 mL). Ether extract was separated, and a saturated solution of NaCl in 2% hydrochloric acid was added dropwise to a stirred ether solution until the pH of water phase decreased to 1 and colored nitroxide completely moved to the water phase. The solution was stirred until the mesylate **12** completely disappeared. The water solution was separated, washed with ether, and basified with $NaHCO_3$. The basified mixture was again extracted with diethyl ether, the combined extracts were dried with Na_2CO_3, the solvent was removed under reduced pressure, and the residue was separated using column chromatography on silica gel, eluent $CHCl_3$. The isolated nitroxide was converted into chlorohydrate by carefully dissolving in 2% HCl and evaporating under reduced pressure. Yield 890 mg (78%).

Hydrophilic Spin Probe Im6

2-(4-((2-(4-Amino-4-carboxybutanamido)-3-(carboxymethylamino)-3-oxoproylthio)-methyl)phenyl)-4-pyrrolidino-2,5,5-triethyl-2,5-dihydro-1Himidazol-1-oxyl-D_{11} (**Im6**) was synthesized as follows. A solution of a spin label **RCl** (62.5 mg, 156.5 μmol) in methanol (1 mL) was added dropwise under argon to a solution of glutathione (58.7 mg, 191.0 μmol) and NaOH (30.5 mg, 762.5 μmol) in methanol (5 mL). The reaction mixture was stirred overnight under argon and then neutralized by addition of HCl followed by evaporation. The

residue was dissolved in 3 mL of H_2O, and pH was adjusted to 5.2 by addition of HCl or NaOH. The solution was placed on C18 SPE column (HyperSep, Thermo Scientific) and washed with 10 mL of H_2O. The product was eluted from the column with 30% methanol. After evaporation, the spin probe **Im6** was obtained, yield 94.2 mg (95%). Mass spectrum of the **Im6**-$\mathbf{H}^+$ (M^+): calcd for $C_{30}H_{37}D_9N_6O_7S$ 643.3704 (R = CH_3, see Scheme 1), found 643.3726; calcd for $C_{30}H_{34}D_{12}N_6O_7S$ 646.3890 (R = CD_3), found 646.3892.

pH Calibration of Im6 Probe Using EPR Spectroscopy

Solutions of 0.5 mM nitroxide **Im6** in a 2 mM Na-phosphate buffer, 150 mM NaCl were titrated with aliquots of HCl or NaOH to the required pH using a pH meter. EPR spectra of the samples were recorded in 1.5 mL centrifuge tubes using an L-band EPR spectrometer (Magnettech, Germany). Nitrogen hyperfine splitting constant (a_N) was calculated as a half of the distance between low- and high-field spectral components. Temperature control was performed using a water bath attached to the thermostat.

pH Calibration of Im6 Probe Using PEDRI

pH calibration was performed by variable radio frequency (VRF) PEDRI of the phantom consisting of 10 tubes: 9 tubes were filled with a 1 mM solution of the probe prepared at different pH values from 4.5 to 8.2; the 10th tube was filled with water to be used as a reference. Two PEDRI acquisitions at EPR irradiation frequencies, RF_1 = 562.1 MHz and RF_2 = 559.3 MHz, and one MRI image were obtained. EPR frequencies were equidistant by ±1.4 MHz (±0.5 G) from the central frequency of the resonator, 560.7 MHz. EPR *off* image was subtracted from both EPR *on* images acquired at two EPR frequencies, yielding image intensities $I(RF_1)$ and $I(RF_2)$. Then, the ratio $I(RF_1)/(I(RF_1) + I(RF_2))$ was calculated for each pixel, averaged in each of the tubes, and plotted as a function of pH.

PEDRI Instrument

A custom-built PEDRI instrument has been used to perform VRF PEDRI experiments at 0.02 T magnetic field. Water-cooled iron core Resonex 5000/Paradigm resistive magnet (Resonex Corp., Sunnyvale, CA) with a gap of 50 cm between the magnet poles and powered by modified Danfysik MPS 854/SYS 8000 power supply was used to generate the field. High homogeneity of the NMR field, better than 20 ppm over a 25 cm × 20 cm × 20 cm volume, was achieved using 24 active shims. A high stability of the current and, therefore, of the magnetic field (better than 0.5 ppm/h) was achieved by a high precision manually adjustable reference voltage. The EPR transmit system is based on a Alderman-Grant resonator with capacitive coupling in combination with a solenoidal coil for the NMR channel.[30] The EPR excitation signal was generated by an externally triggered Fluke 6089A frequency synthesizer and amplified by a Kalmus 7150LC power amplifier (Amplifier Research, Souderton, PA).

Fast Spin Echo (FSE) Sequence

For PEDRI experiments, a 2D FSE pulse sequence (MR Solutions Inc.) was used (see the Supporting Information).[19] EPR irradiation was applied to the EPR resonator 400 ms before the application of the FSE pulse sequence and maintained during image acquisition. Single slice images were acquired using the 2D FSE pulse sequence and the following parameters: TR = 2 s, base TE = 30 ms, effective TE = 150 ms, views per segment =16, slice thickness = 20 mm, field of view (FOV) = 100 mm × 100 mm, matrix size = 64 × 64, number of average = 1, scan time = 8.4 s. Images were acquired with EPR frequencies, RF_1 = 562.1 MHz and RF_2 = 559.3 MHz; NMR frequency, 784.9 kHz, incident EPR rf power, 40 W.

Probe Cytotoxicity Studies

Cytotoxicity of **Im6** probe on Met-1 mouse breast cancer cells, MDA-MB-231 human breast cancer cells, and MCF10A normal human mammary epithelial cells were performed using the XTT Cell Viability Assay. Met-1 and MDA-MB-231 cells were cultured in DMEM media containing 10% fetal bovine serum (FBS) and 1% penicillin/streptomycin/amphotericin B (PSA). MCF10A cells were cultured in DMEM/F12 media containing 5% FBS, 20 μg/ mL EGF, 0.1 μg/mL hydrocortisone, 10 μg/mL insulin, and 1% PSA. All cells were plated in a 96-well plate at 2.5×10^4 cells per well in 200 μL of media. After adherence, the **Im6** probe was resuspended in PBS and added at 0, 0.1, 1.0, or 5.0 mM. After 24 h incubation at 37 °C and 5% CO_2, 50 μL of XTT assay reagents was mixed as per the manufacturer instructions (Roche, catalog no. 11465015001) and added to each well and returned to 37 °C and 5% CO_2 for 4 h. The plate was analyzed at 450 nm (primary wavelength) and 630 nm (reference wavelength) as per the manufacturer instructions. The data is reported as percent cell proliferation of each cell line relative to its own 0 probe condition. All samples were performed in quadruplicate.

In Vivo Experiments

C57Bl/6 background Met-1 murine breast cancer cells were expanded in DMEM containing 10% fetal bovine serum, 10 μg/mL insulin, 5 ng/mL rhEGF, and 1% PSA (penicillin G sodium, streptomycin sulfate, and amphotericin B) then trypsinized, washed, and loaded into insulin syringes at 1×10^6 cells per 100 μL. The tumor cells were implanted into the number 4 mammary fat pads of 8-week-old female C57Bl/6 wild type mice (Jackson Laboratory). After the tumors became palpable (approximately 3 weeks), tumor dimensions were measured one time per week using calipers and tumor volumes were calculated using the equation: volume = $(\text{width}^2) \times (\text{length}/2)$. PEDRI measurements were performed on normal mammary glands and untreated Met-1 tumors with an average tumor volume of 0.5 cm^3 in the mice (number of animals, $n = 3$) anesthetized by inhalation of a mixture of oxygen with isoflurane using an Ohmeda Fluotec 3 anesthetic machine. Solutions of the pH probe in saline (50 μL, 5 mM) was injected into the number 4 mammary gland and into the number 9 normal mammary gland before PEDRI/MRI acquisition. Mice were placed into the PEDRI resonator assembly followed by tuning of the resonators and PEDRI acquisition as described in the previous section. Only pixels with signal intensity exceeding 20% from the maximal intensity were used for pH mapping. Image acquired in the absence of EPR irradiation was subtracted from images acquired at two EPR irradiation frequencies, and the obtained images were divided pixel by pixel. A resulted pixel-specific ratio was converted to a pH map using the VRF PEDRI pH calibration curve obtained as described above. All animal work was performed in accordance with the OSU IACUC approved protocol.

Validation of VRF PEDRI pH Measurements

VRF PEDRI and electrochemical pH measurements were performed in wild type C57Bl/6 mice on normal mammary glands and untreated Met-1 tumors with the average tumor volume of 0.5 cm^3. A pH microelectrode (Warner Instr. Hamden, CT) was placed into the tumors or mammary glands using a 20 gauge needle. Tissue pH values were measured electrochemically during 3 min interval, immediately followed by VRF PEDRI pH mapping.

Phantom and Tissue Temperature Measurements

Temperature was measured using a Nomad fiber optic thermometer (Neoptix, Canada) equipped with a fiber optic sensor with a probe diameter of 0.5 mm and precision ±0.2 °C. Temperature measurements performed with a phantom simulating mouse[18] suggest that body temperature increase does not exceed 1 °C during 17 s of continuous rf irradiation. In the case of *in vivo* experiments, the sensor was inserted into the mammary gland or

mammary tumor using a sterile, stainless steel needle (gauge 18). To eliminate still-induced heat loss and interference with rf, the needle was then removed leaving the sensor in the tissue at about 3 mm depth from the surface.

RESULTS AND DISCUSSION

Optimization of pH Probe Structure for PEDRI Assessment of Extracellular Tumor pH

Extracellular tumor pH is a prognostic factor in tumor pathophysiology.[11] As follows from the previous section, to perform PEDRI pH mapping of living tissue using nitroxide pH probes requires an increase of the probe pK_a value and half-life, *in vivo*. In addition, for tumor pH_e monitoring, a membrane-impermeable probe should be used to ensure extracellular localization.

As one can see from Table 1, the pK_a values of 4-amino-2,5-dihydroimidazol-1-oxyl derivatives (**Im2**–**Im4**) are much closer to the physiological range of pH than pK_a of **In** derivatives. The pK_a values of these nitroxides are dependent upon the electronic character of the substituents at the basic amidine moiety. It has been shown that 4-dialkylamino-2,2,5,5-tetraalkyl-2,5-dihydroimidazol-1-oxyls, i.e., nitroxides with electron-donating alkyl substituents both at the exocyclic nitrogen atom and in the positions 2 and 5 of the imidazole ring, have a pK_a value close to 7.[31,32] It was also found that 4-pyrrolidino-derivatives are more basic than di-*n*-alkylamino- or piperidino-group-containing compounds.[4,31,33]

The bulky alkyl substituents adjacent to the nitroxide group have been shown to be an efficient method to decrease the rate of nitroxide reduction with low-molecular biogenic antioxidants, e.g., ascorbate.[32] To ensure cell-impermeable properties, the introduction of a hydrophilic substituent in the nitroxide structure can be performed. The binding of hydrophilic tripeptide, GSH, to the labeling group of the nitroxide efficiently prevents probe diffusion across the lipid bilayer of the biomembranes[33,34] and, therefore, can be used to maintain probe localization in the extracellular aqueous environment. However, it is known that introduction of alkylating- or acylating-labeling groups in the side chain of 4-amino-2,5-dihydroimidazol-1-oxyl derivatives usually leads to intramolecular alkylation or acylation of the amidine moiety with a loss of sensitivity to pH in the desired region.[35] Fortunately, it has been found that the derivatives containing a 4-(chloromethyl)phenyl labeling group (e.g., the nitroxide **RCl**, Scheme 1) do not permit intramolecular alkylation and can be prepared as stable labels. Following this strategy, the nitroxide **Im5** (Figure 1) has been recently synthesized.[2] The electron-donating properties of the 4-pyrrolidino group results in the pK_a value of **Im5** being close to 7. Bulky ethyl substituents in positions 2 and 5 of the radical heterocycle increase probe stability toward reduction by an order of magnitude while binding to highly hydrophilic glutathione tripeptide ensures probe extracellular localization. The nitroxide **Im5** has proven to be a useful probe for EPR *in vivo* monitoring of tumor tissue acidosis.[2]

PEDRI applications require a paramagnetic probe with a narrow line width to obtain a high enhancement and decrease rf power deposition. Our attempts to use the **Im5** probe for *in vivo* PEDRI pH mapping failed due to low signal enhancement as a consequence of a comparatively large line width, ΔH_{pp} = 2.1 G. Recent EPR and quantum-chemical studies showed that major contribution into the line width of tetraethyl-substituted imidazoline nitroxides comes from unresolved super hyperfine splitting of methylene protons of ethyl groups.[28] Therefore, in our work to decrease probe line width, we synthesized the partially deuterated analogue of the **Im5**, namely, nitroxide **Im6** (Scheme 1) substituting all methylene protons with deuterium isotopes as described in the Materials and Methods.

Figure 1 illustrates the EPR spectra of the probes **Im5** and **Im6** confirming a significantly narrower line width (ΔH_{pp} = 1.2 G) and therefore about a 3-fold higher signal amplitude of the deuterated probe. At intermediate pH close to the pK_a value, the EPR spectrum of **Im6** (Figure 1d) shows the superposition of unprotonated, R, and protonated, RH^+, forms in agreement with slow proton exchange between these forms on the L-band EPR time scale.[36] The ratio of concentrations of these two forms is described by the Henderson–Hasselbalch equation, $[H^+] = K_a[RH^+]/[R]$, providing the basis for pH assessment using the spin pH probe (see Figure 2a). One of the advantages of the approach is that it is ratiometric, the pH measurement being dependent on the concentration ratio, $[RH^+]/[R]$ but independent of the absolute probe concentration. Note that Lband EPR spectra of the R and RH^+ forms are partially overlapped (Figure 1d) which allows for pH calibration of apparent nitrogen hyperfine splitting, a_N(pH), measured as a distance between low- and high-field spectral components (Figure 2b). The a_N hyperfine splitting has been widely used as a pH-sensitive parameter in previous *in vivo* EPR applications of the nitroxides.[2,18,23,25,37,38] The dependence a_N(pH) deviates from the conventional titration curve when the splitting between R and RH^+ is larger or comparable to the EPR line width (Figure 2b, circles). This deviation can be avoided by spectra acquisition at higher modulation amplitude[39] due to the corresponding line broadening (Figure 2b, squares). The observed pK_a value of **Im6** and the range of pH sensitivity (Figure 2) ideally fit for assessment of extracellular pH in solid tumors.

Nitroxides are considered remarkably nontoxic being used in human studies[40] and in several clinical trials as antioxidants. We expect the newly synthesized, highly hydrophilic membrane-impermeable nitroxide **Im6**, specially designed to remain in the extracellular tissue microenvironment, to have minimal toxicity, if any. To test the **Im6** probe for cell cytotoxicity, we performed the XTT cell viability assay on the Met-1 mouse tumor cells. To determine any toxicity effects of **Im6** on human tumor or normal mammary cells, we performed the XTT assay on MDA-MB-231 human breast cancer cells and MCF10A normal human mammary epithelial cells. No toxicity of probe in concentrations up to 5 mM was observed. Note that estimated concentrations of the **Im6** probe used in further PEDRI experiments *in vivo* were about 0.5 mM.

VRF PEDRI pH Mapping Using Im6 Nitroxide Probe: Phantom Studies

Figure 3 illustrates the concept of VRF PEDRI application to pH mapping using the pH-sensitive probe. Protonation of the pH probes **Im5** and **Im6** results in about a 1 G shift of the high-field spectral component due to a corresponding decrease of nitrogen hyperfine splitting (see Figure 2b). This field shift is transformed to about a 3 MHz frequency shift from $RF_1 \approx 562$ MHz to $RF_2 \approx 559$ MHz for the experiment at a fixed magnetic field of 200 G which corresponds to a proton NMR frequency of 783 kHz. The ratio of the MRI enhancements obtained upon EPR irradiations at RF_2 and RF_1 frequencies reflects the $[RH^+]/[R]$ ratio, therefore providing basis for PEDRI pH assessment. To maintain the same EPR power at both rf irradiations, the resonator must be tuned to the frequency which is equidistant from RF_1 and RF_2. The *Q* factor of the sample-loaded resonator is approximately 200 meaning that a shift from the central frequency by 1.5 MHz leads to a decrease in the EPR rf irradiation power by less than 50% within the sample. This corresponds to an ~1.4-fold reduction in enhancement. Fine tuning of the frequencies RF_1 and RF_2 were achieved by maximizing MRI enhancements of the samples with completely protonated (pH ~ 4) and unprotonated (pH ~ 8) nitroxides giving for **Im5** and **Im6** the values of RF_1 and RF_2 listed in the Figure 3 caption. Note that comparative VRF PEDRI phantom studies of **Im5** and **Im6** probes demonstrated about 4-fold higher enhancements for the deuterated analogue **Im6** (data not shown) which is of critical importance for *in vivo* experiments.

Figure 4 represents the calibration of VRF PEDRI using the **Im6** probe on pH obtained using a 10-tube phantom (Figure 4a) containing the samples titrated to different pH values. EPR frequencies were preselected as illustrated in Figure 3. A fast spin echo sequence has been applied with an acquisition time of 8.4 s for each image (Figure 4b,c). The EPR *off* image was subtracted from both EPR *on* images acquired at RF_1 and RF_2, yielding image intensities, $I(RF_1)$ and $I(RF_2)$, respectively. The pH dependence of intensities ratio $I(RF_1)/(I(RF_1) + I(RF_2))$ shown in Figure 4d (see Materials and Methods for details) is described by the titration curve with the observed pK_a value of **Im6** probe equal to 6.75 ± 0.05 in agreement with the EPR-measured pK_a value, 6.74 ± 0.05 (Figure 2a).

In Vivo VRF PEDRI pH Mapping Using Im6 Nitroxide Probe

In general, quantitative determination of pH in live animals requires calibration of the pH probe at tissue temperature. The tissue temperatures measured both in normal mammary glands and tumors using a microsensor (see the Materials and Methods) were found to be slightly lower (33.5–34.5 °C) compared to the average temperature of mouse body (37 °C), which might be a consequence of the underdeveloped microcirculation and tissue proximity to the surface. The performed pH titration of the **Im6** probe at 34 °C demonstrated a small decrease from the pK_a value measured at 23 °C of about 0.06 units (see Figure 2). Therefore, the calibration curve (Figure 4d) used for *in vivo* PEDRI pH calculations was shifted by 0.06 pH units to reflect a temperature-induced pK_a shift from the pK_a = 6.75 measured at room temperature (Figure 4d) to the expected pK_a = 6.69 at 34 °C.

The *in vivo* PEDRI measurements were performed on untreated Met-1 tumors with an average tumor volume of 0.5 cm^3 and normal mammary glands in anesthetized wild type C57Bl/6 mice immediately after intratissue **Im6** probe injection (see Materials and Methods). An improved probe stability toward reduction resulted in sufficiently long half-lives of the probe of about 3 min in tumor tissue and more than 10 min in mammary gland allowing for accurate PEDRI acquisitions (8 s per image, see Figure 5). The shorter half-live of the probe in tumor compared with mammary gland is in agreement with the higher reducing capacity of the tumor tissue.[2] Figure 5a shows an MRI image acquired with EPR irradiation, therefore demonstrating probe distribution. The probe distribution area in tumor is about 1 cm^2, which is close to the value of tumor cross-section area (the measured tumor size is about 1.2 cm × 0.9 cm), therefore supporting probe localization within the tumor. The probe distribution area in the mammary gland is less than 0.2 cm^2 being close to its size. Figure 5b shows the pH map (in color) superimposed with low-field MRI (gray scale) representing the coronal view of the mouse. The pH map was computed from the pixel-wise intensities of PEDRI images acquired during EPR irradiation at frequencies RF_1 and RF_2, using a calibration curve. The broader pH_e distribution in tumor in the range from 6.4 to 7.1 compared with pH_e distribution in mammary gland from pH 7.0 to 7.2 was observed in agreement with high heterogeneity of the tumor microenvironment. Average values of pH_e in tumor and mammary gland were found to be 6.8 ± 0.1 and 7.1 ± 0.1, respectively, supporting significant tumor tissue acidosis. The averaged pH values measured by PEDRI and pH microelectrode coincide within the 0.1 pH unit further validating the PEDRI approach.

CONCLUSIONS

The VRF PEDRI approach for *in vivo* pH mapping using a specially designed nitroxide probe has been applied to studies of tumor tissue acidosis in live mice. The developed method may be a useful tool for spatially resolved noninvasive extracellular pH monitoring in solid tumors in preclinical studies on small animals. Moreover, MRI-based PEDRI pH

mapping using nitroxide probes has a potential to be used in larger animals, including humans.

Supplementary Material

Refer to Web version on PubMed Central for supplementary material.

Acknowledgments

This work was partly supported by NIH Grants EB014542 and EB016096, the Russian Foundation for Basic Research, Grants 12-03-00718-a and 12-03-00737-a, and the Ministry of Education and Science of the Russia Federation, Grant 8456.

REFERENCES

1. Zhang X, Lin Y, Gillies RJ. J. Nucl. Med. 2010; 51:1167–1170. [PubMed: 20660380]
2. Bobko AA, Eubank TD, Voorhees JL, Efimova OV, Kirilyuk IA, Petryakov S, Trofimiov DG, Marsh CB, Zweier JL, Grigor'ev IA, Samouilov A, Khramtsov VV. Magn. Reson. Med. 2012; 67:1827–1836. [PubMed: 22113626]
3. Niwano S, Tojo T. Circ. J. 2010; 74:1794–1795. [PubMed: 20702957]
4. Komarov DA, Dhimitruka I, Kirilyuk IA, Trofimiov DG, Grigor'ev IA, Zweier JL, Khramtsov VV. Magn. Reson. Med. 2012; 68:649–655. [PubMed: 22162021]
5. Kraig RP, Petito CK, Plum F, Pulsinelli WA. J. Cereb. Blood Flow Metab. 1987; 7:379–386. [PubMed: 3611202]
6. Woitzik J, Back T, Thome C. Front. Biosci. 2008; 13:1500–1506. [PubMed: 17981644]
7. Ichiwata T, Sasao G, Abe T, Kikuchi K, Koyama K, Fujiwara H, Nagai A, Kuwahira I, Nagao K. Adv. Exp. Med. Biol. 2010; 662:537–543. [PubMed: 20204842]
8. Kraut JA, Madias NE. Pediatr. Nephrol. 2011; 26:19–28. [PubMed: 20526632]
9. Wang L, Li C. J. Mater. Chem. 2011; 21:15862–15871.
10. Vavere AL, Biddlecombe GB, Spees WM, Garbow JR, Wijesinghe D, Andreev OA, Engelman DM, Reshetnyak YK, Lewis JS. Cancer Res. 2009; 69:4510–4516. [PubMed: 19417132]
11. Gillies RJ, Raghunand N, Garcia-Martin ML, Gatenby RA. IEEE Eng. Med. Biol. Mag. 2004; 23:57–64. [PubMed: 15565800]
12. Gallagher FA, Kettunen MI, Day SE, Hu DE, Ardenkjaer-Larsen JH, Zandt R, Jensen PR, Karlsson M, Golman K, Lerche MH, Brindle KM. Nature. 2008; 453:940–943. [PubMed: 18509335]
13. Khramtsov VV. Curr. Org. Chem. 2005; 9:909–923.
14. Koda S, Goodwin J, Khramtsov VV, Fujii H, Hirata H. Anal. Chem. 2012; 84:3833–3837. [PubMed: 22424377]
15. Lurie DJ, Bussell DM, Bell LH, Mallard JR. J. Magn. Reson. 1988; 76:366–370.
16. Overhauser AW. Phys. Rev. 1953; 92:411–415.
17. Lurie DJ, Nicholson I, Foster MA, Mallard JR. Phil. Trans. R. Soc. London, Ser. A: Math. Phys. Eng. Sci. 1990; 333:453–456.
18. Potapenko DI, Foster MA, Lurie DJ, Kirilyuk IA, Hutchison JM, Grigor'ev IA, Bagryanskaya EG, Khramtsov VV. J. Magn. Reson. 2006; 182:1–11. [PubMed: 16798033]
19. Sun Z, Li H, Petryakov S, Samouilov A, Zweier JL. J. Magn. Reson. Imaging. 2012; 35:471–475. [PubMed: 22147559]
20. Krishna MC, English S, Yamada K, Yoo J, Murugesan R, Devasahayam N, Cook JA, Golman K, Ardenkjaer-Larsen JH, Subramanian S, Mitchell JB. Proc. Natl. Acad. Sci. U.S.A. 2002; 99:2216–2221. [PubMed: 11854518]
21. Khramtsov VV, Caia GL, Shet K, Kesselring E, Petryakov S, Zweier JL, Samouilov A. J. Magn. Reson. 2010; 202:267–273. [PubMed: 20007019]

22. Efimova OV, Sun Z, Petryakov S, Kesselring E, Caia GL, Johnson D, Zweier JL, Khramtsov VV, Samouilov A. J. Magn. Reson. 2011; 209:227–232. [PubMed: 21320790]
23. Khramstov, VV. Nitroxides - Theory, Experiment and Applications. Kokorin, AI., editor. Rijeka, Croatia: InTech; 2012. p. 317-346.
24. Khramtsov VV, Grigor'ev IA, Foster MA, Lurie DJ, Nicholson I. Cell. Mol. Biol. 2000; 46:1361–1374. [PubMed: 11156481]
25. Foster MA, Grigor'ev IA, Lurie DJ, Khramtsov VV, McCallum S, Panagiotelis I, Hutchison JM, Koptioug A, Nicholson I. Magn. Reson. Med. 2003; 49:558–567. [PubMed: 12594760]
26. Khramtsov VV, Weiner LM, Grigor'ev IA, Volodarsky LB. Chem. Phys. Lett. 1982; 91:69–72.
27. Khramtsov, VV.; Komarov, DA. Nanomedicine and the Cardiovascular System. Hunter, RJ.; Preedy, VR., editors. Enfield, NH: Science Publishers and CRC Press; 2011. p. 200-220.
28. Bobko AA, Kirilyuk IA, Gritsan NP, Polovyanenko DN, Grigor'ev IA, Khramtsov VV, Bagryanskaya EG. Appl. Magn. Reson. 2010; 39:437–451. [PubMed: 22162912]
29. Kirilyuk IA, Morozov DA, Tabatchikova YS, Medvedev VS, Lebedev AV, Romanenko GV, Rybalova TV, Grigorrev IA. Russ. Chem. Bull. 2008; 57:1516–1533.
30. Petryakov S, Samouilov A, Roytenberg M, Li H, Zweier JL. Magn. Reson. Med. 2006; 56:654–659. [PubMed: 16902975]
31. Kirilyuk IA, Shevelev TG, Morozov DA, Khromovskih EL, Skuridin NG, Khramtsov VV, Grigor'ev IA. Synthesis. 2003:871–878.
32. Kirilyuk IA, Bobko AA, Grigor'ev IA, Khramtsov VV. Org. Biomol. Chem. 2004; 2:1025–1030. [PubMed: 15034626]
33. Woldman YY, Semenov SV, Bobko AA, Kirilyuk IA, Polienko JF, Voinov MA, Bagryanskaya EG, Khramtsov VV. Analyst. 2009; 134:904–910. [PubMed: 19381383]
34. Khramtsov VV, Panteleev MV, Weiner LM. J. Biochem. Biophys. Methods. 1989; 18:237–246. [PubMed: 2543696]
35. Polienko JF, Sching T, Gatilov Y, Grigor'ev I, Voinov M. J. Org. Chem. 2008; 73:502–510. [PubMed: 18085792]
36. Khramtsov VV, Weiner LM, Eremenko SI, Belchenko OI, Schastnev PV, Grigor'ev IA, Reznikov VA. J. Magn. Reson. 1985; 61:397–408.
37. Mader K, Gallez B, Liu KJ, Swartz HM. Biomaterials. 1996; 17:457–461. [PubMed: 8938242]
38. Gallez B, Mader K, Swartz HM. Magn. Reson. Med. 1996; 36:694–697. [PubMed: 8916019]
39. Khramtsov VV, Grigor'ev IA, Foster MA, Lurie DJ. Antioxid. Redox Signal. 2004; 6:667–676. [PubMed: 15130294]
40. He G, Samouilov A, Kuppusamy P, Zweier JL. J. Magn. Reson. 2001; 148:155–164. [PubMed: 11133289]

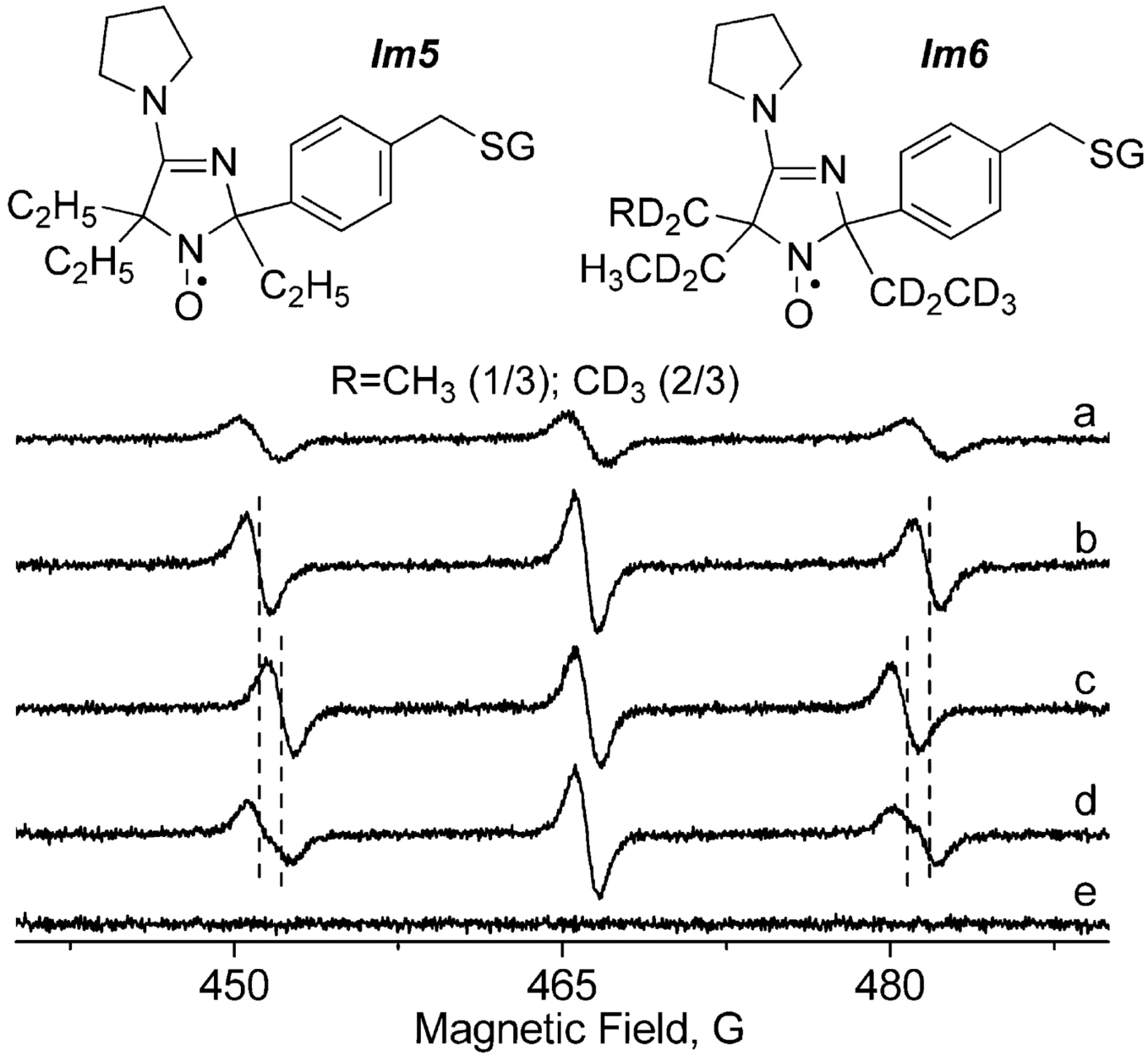

Figure 1.

Chemical structures and L-band EPR spectra of the pH-sensitive imidazoline nitroxides, **Im5** (a) and **Im6** (b–e). The 0.5 mM solutions of the nitroxides were prepared in 2 mM Na-phosphate buffer, 150 mM NaCl, pH 9.8 (a, b), 4.5 (c), and 6.8 (d) and measured at 23 °C. Trace e represents the subtraction of the EPR spectrum (trace d) from the weighted sum of the EPR spectra (trace b, 53%) and (trace c, 47%). A dashed line is extended from the center of each line of the spectra (traces b and c) to aid the eye. Acquisition parameters were: sweep width, 60 G; modulation amplitude, 0.5 G; one scan, time 20 s; number of points, 2048.

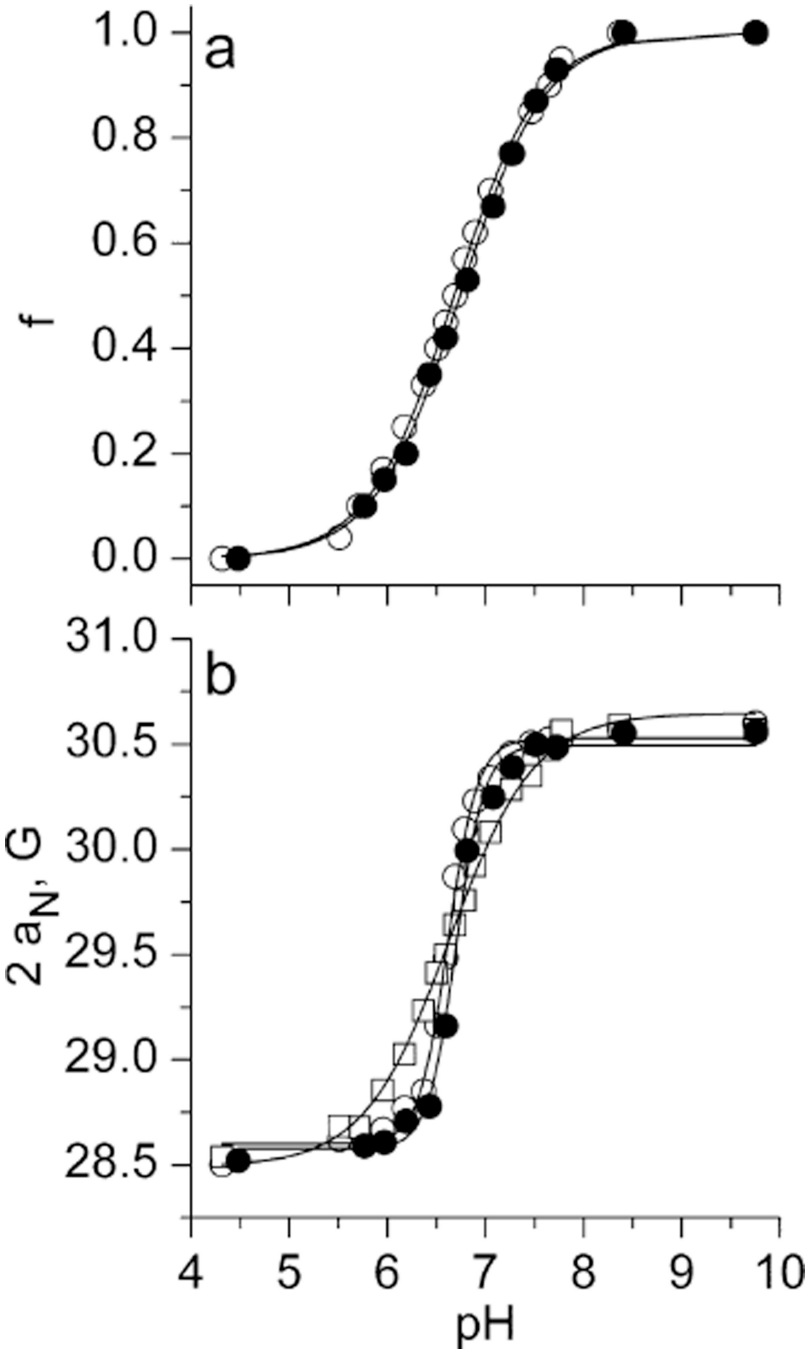

Figure 2.

(a) The pH dependencies of the fraction of the unprotonated form of the nitroxide **Im6** calculated from the EPR spectra measured at 23 °C (●) and 34 °C (○). Solid lines represent the best fits of the experimental data to the conventional titration equation, $f = 1/(1 + [H^+]/K_a)$, yielding pK_a values equal to 6.74 ± 0.05 (23 °C) and 6.68 ± 0.05 (34 °C). (b) The pH dependencies of hfs, $2a_N$, between low- and high-field components of the EPR spectra measured at 23 °C (●) and 34 °C (○ and □) using the value of modulation amplitude 0.5 G (● and ○) and 2.5 G (□). Solid lines represent the best fits of the experimental data to the equation $2a_N(pH) = (2a_N(R) + 2a_N(RH^+) \times ([H^+]/K_a)^d)/(1 + ([H^+]/K_a)^d)$ yielding pK_a values

6.70 ± 0.05 (23 °C) and 6.64 ± 0.05 (34 °C). The parameter *d* reflects the degree of deviation of the dependence a_N(pH) from the conventional titration curve (*d* = 1) being equal to 3.0 and 1.0 for the dependencies obtained at low, 0.5 G, and high, 2.5 G, modulation amplitudes, correspondingly.

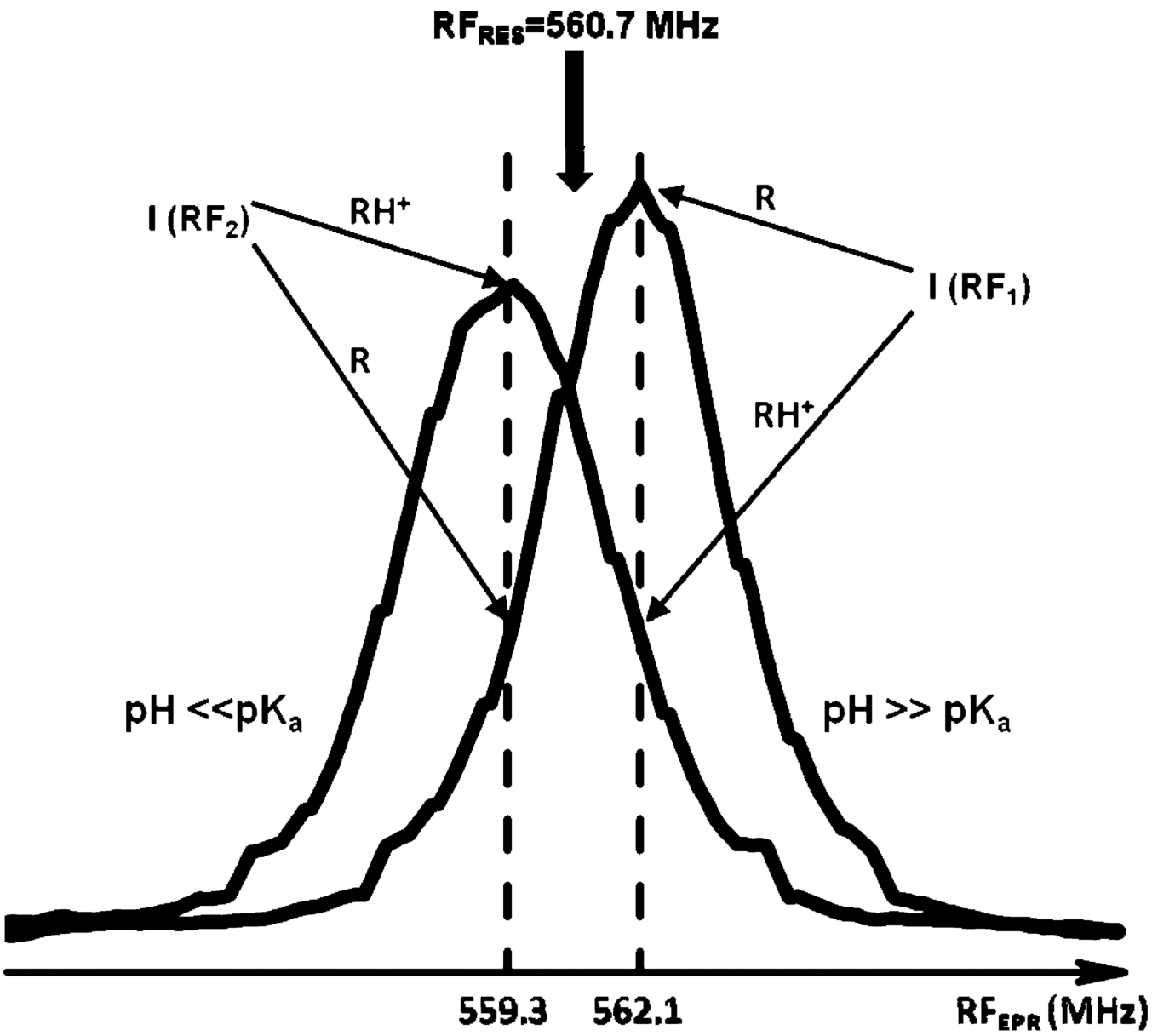

Figure 3.

VRF PEDRI approach to pH mapping. RF_1 and RF_2 are EPR radio frequencies corresponding to the centers of the high field EPR component of the unprotonated, R, and protonated, RH^+, forms of the radical, respectively. The resonator is tuned to the frequency equidistant from RF_1 and RF_2. For the probes **Im5** and **Im6**, RF_1 = 562.1 MHz; RF_2 = 559.3 MHz; EPR resonator frequency, 560.7 MHz; NMR frequency, 784.9 kHz.

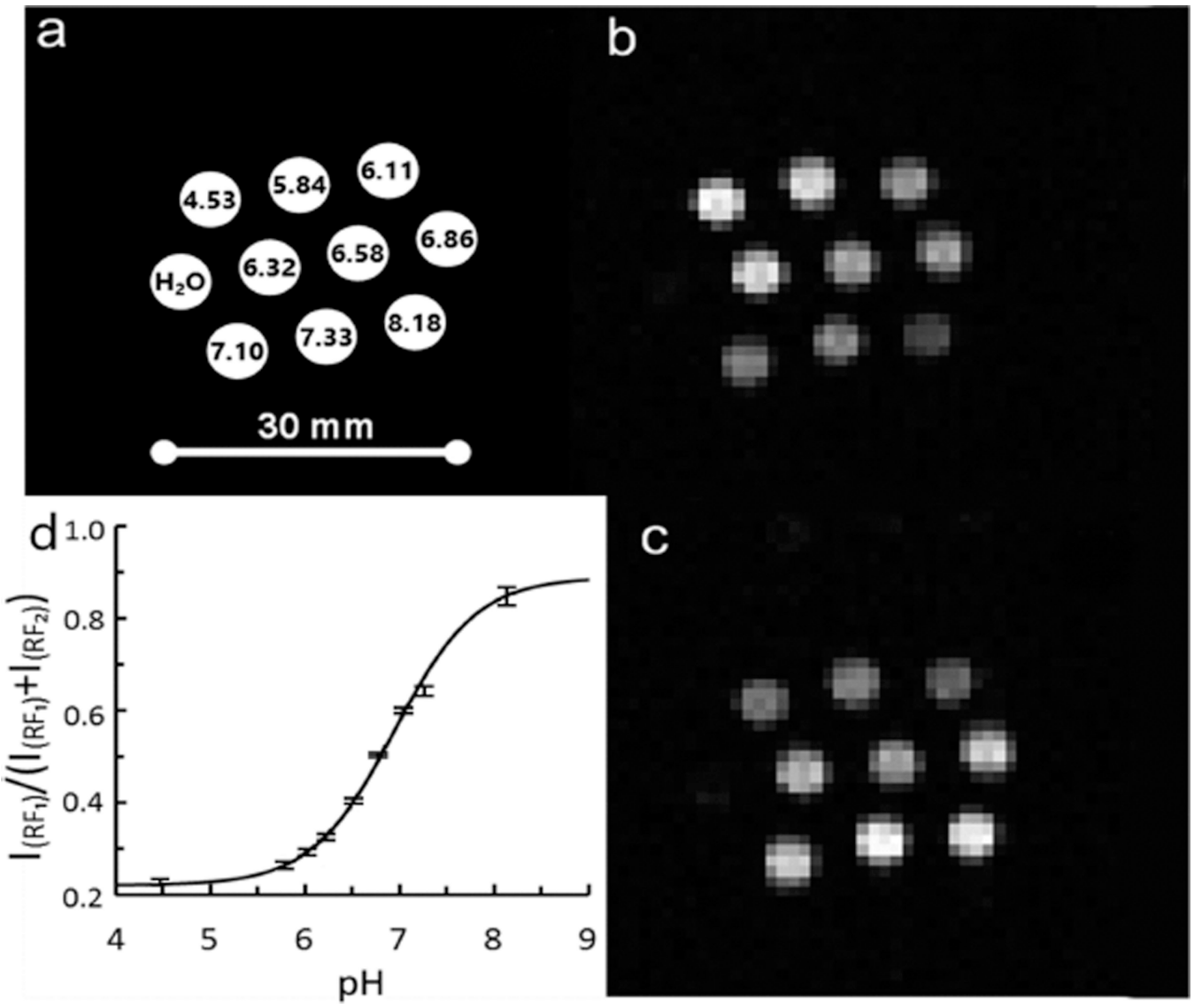

Figure 4.

Calibration of VRF PEDRI of the **Im6** probe on pH obtained using 10-tube phantom (a) at room temperature. PEDRI images were acquired at RF_2 = 559.3 MHz (b) and RF_1 = 562.1 MHz (c), acquisition time of 8.4 s. The tube with water alone is not visible on either image due to lower intensity compared to signal from tubes containing paramagnetic probe. EPR *off* image (not shown) was subtracted from both EPR *on* images acquired at RF_1 and RF_2, yielding image intensities, $I(RF_1)$ and $I(RF_2)$. (d) pH dependence of the ratio $I(RF_1)/(I(RF_1) + I(RF_2))$. The solid line is nonlinear least-squares fit of the data to a conventional titration equation yielding a pK_a value equal to 6.75 ± 0.05. Error bars represent the standard deviation.

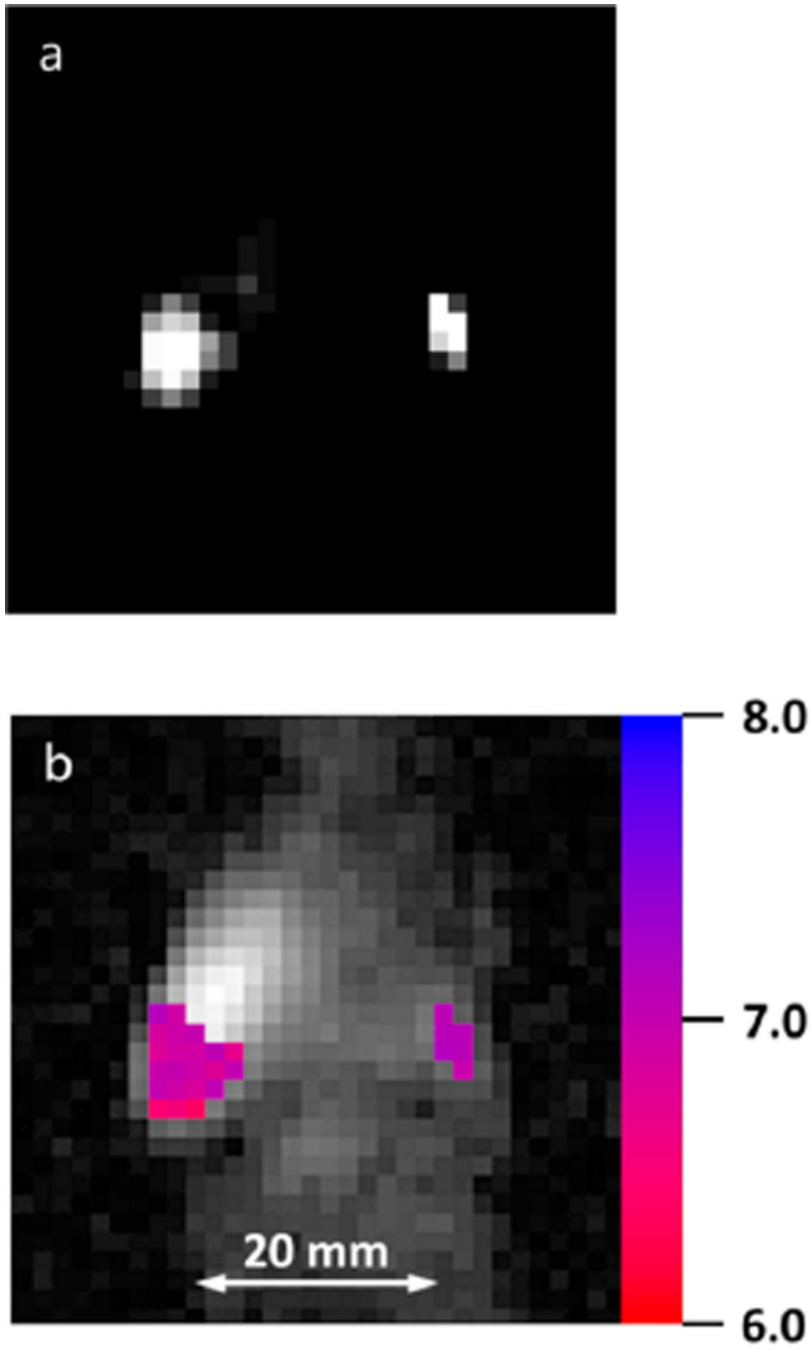

Figure 5.

PEDRI pH mapping in living mice. Paramagnetic **Im6** probe was injected into the tumor (number 4 mammary gland, left) and normal mammary gland (number 9, right). (a) Qualitative visualization of the distribution of the **Im6** probe, *in vivo*. The image is the average of two PEDRI images acquired at two EPR frequencies, RF_1 = 562.1 MHz and RF_2 = 559.3 MHz. Irradiation time was 8.4 s for each acquisition. (b) Calculated pH map (in color) superimposed with the MRI image (gray scale) showing the coronal view of the mouse. Total acquisition time of pH mapping, 24.8 s; EPR irradiation time, 16.8 s. Presented MRIs were cropped from the images obtained with the following acquisition parameters:

TR, 2 s; TE, 30 ms; matrix, 64 × 64; field of view 100 mm × 100 mm; slice thickness, 20 mm; acquisition time, 8.0 s × 64 averages; NMR frequency, 784.9 kHz.

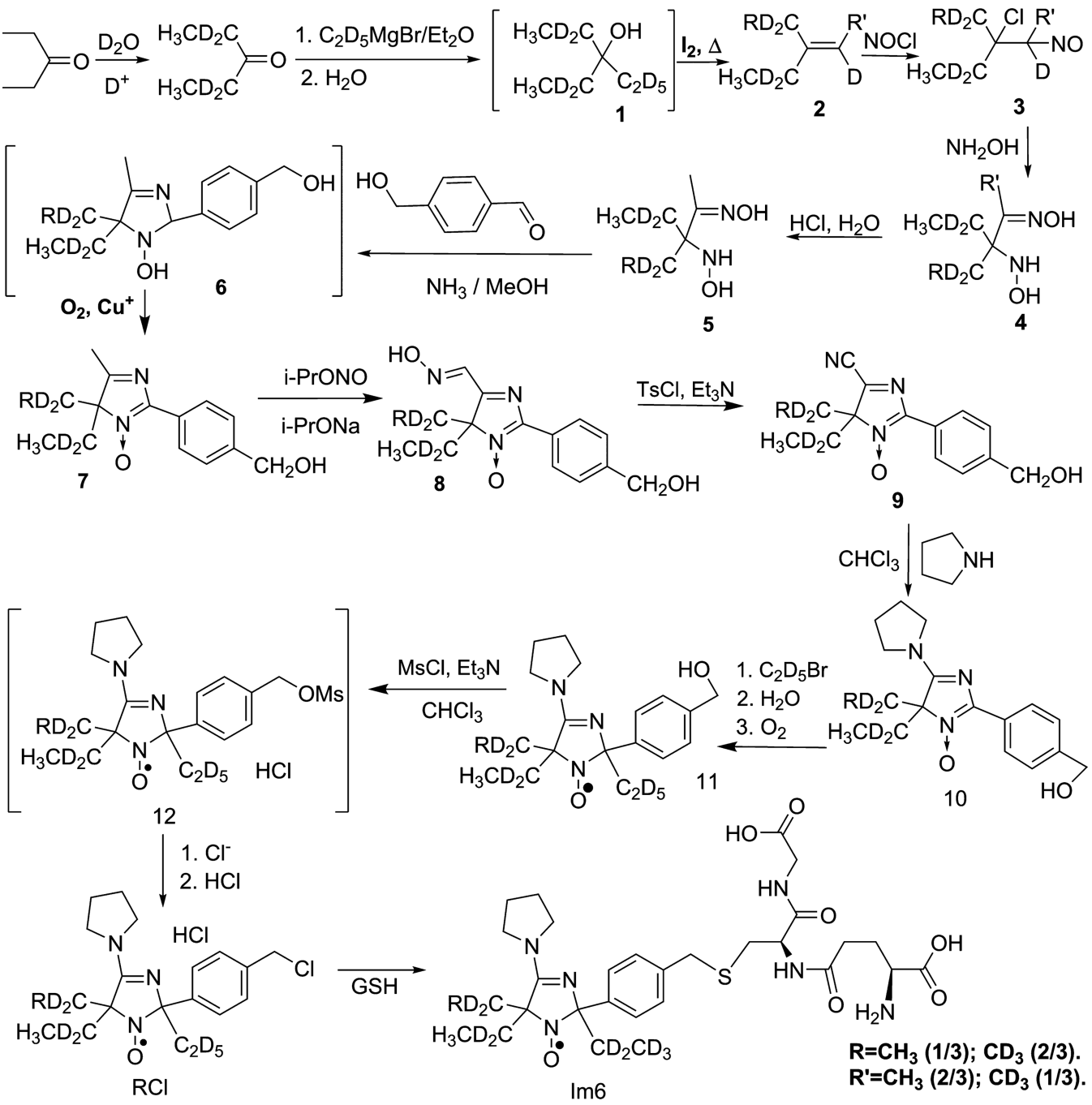

Scheme 1.
Scheme of the Synthesis of Probe Im6

Table 1

pH-Sensitive Nitroxides Previously Used in PEDRI Experiments

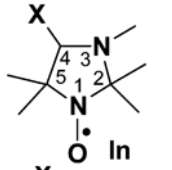

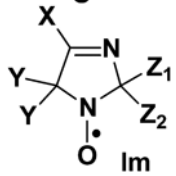

Probe	X	Y	Z_1	Z_2	pK_a, ±0.05[a]
In1[24]	Ph	na	na	na	3.0
In2[24,25]	Me	na	na	na	4.7
Im1[24]	Me	Me	Me	$(CH_2)_2COOH$	1.3
Im2[21,22]	NH_2	Me	Me	Me	6.1
Im3[25]	$N(CH_3)_2$	Me	Et	Py	5.25; 3.1[b]
Im4[25]	$N(CH_2OH)_2$	Et	Et	Py	4.9; 2.8[b]

[a] Measured at room temperature.

[b] pK_a of pyridine group.